Migration of seismicity and earthquake interactions monitored by GPS in SE Asia triple junction: Sulawesi, Indonesia

Christophe Vigny,[1] Hugo Perfettini,[1,2] Andrea Walpersdorf,[1,2] Anne Lemoine,[1] Wim Simons,[3] Danny van Loon,[3] Boudewijn Ambrosius,[3] Colleen Stevens,[4] Rob McCaffrey,[4] Peter Morgan,[5] Yehuda Bock,[6] Cecep Subarya,[7] Parluhutan Manurung,[7] Joenil Kahar,[8,9] Hasanuddin Z. Abidin,[8] and Samad H. Abu[10]

Received 10 July 2000; revised 8 February 2001; accepted 13 February 2001; published XX Month 2002.

[1] Global Positioning System (GPS) measurements made in Sulawesi, Indonesia, from 1992 to 1999 detected coseismic and transient postseismic deformation related to the 1 January 1996, M_w = 7.9 earthquake on the North Sulawesi (Minahassa) trench. These motions are superimposed on the long-term secular motion (40 mm/yr) of the left-lateral Palu fault in central Sulawesi and continued for about 1.5–2 years. Following the earthquake, a string of earthquakes (of magnitude >6) migrated along the Minahassa trench, from west to east. Subsequently, two earthquakes of magnitude >6 occurred on or near the Palu fault migrating toward the south. Modeling the increase in Coulomb stress generated by the successive earthquakes agrees with the hypothesis of interacting events. An unclamping effect, possibly due to fluid migration in the Palu area, is also suggested by the stress computations and the detected (GPS) displacements. *INDEX TERMS:* 1206 Geodesy and Gravity: Crustal movements—interplate (8155); 1242 Geodesy and Gravity: Seismic deformations (7205); 7223 Seismology: Seismic hazard assessment and prediction; 7230 Seismology: Seismicity and seismotectonics; *KEYWORDS:* GPS, fault, fluids, seismotectonics, earthquake, Indonesia

1. Introduction

[2] The Eurasian, Philippine Sea and Australian tectonic plates in SE Asia converge in a complex area of about 500 km diameter in Eastern Indonesia (Figure 1). The tectonics of this area include the Sula block, wedged by the Australian block to the south and the Philippine and Pacific plates to the east. The Sula block moves to the northwest, where shortening occurs by the Sulawesi Sea basin subducting below the northern arm volcanic crust. Sula block motion occurs on two fault systems: the Minahassa subduction thrust running east-west at its northern boundary, and the Palu-Koro strike-slip fault system, roughly running north-south at its western boundary. Rotation of the Sula block around a pole located at the tip of the northern arm of Sulawesi, at a rate of about 4/Myr, produces 40 mm/yr left-lateral almost purely strike-slip motion along the Palu fault [*Walpersdorf et al.*, 1998a; *Stevens et al.*, 1999].

[3] Magnitude ($M_w > 6$) earthquakes since 1 January 1996 from the Harvard centroid moment tensor (CMT) catalog [*Dziewonski et al.*, 1981, 1996 and references therein] for the Sulawesi area reveal propagation of seismicity (Table 1 and Figure 1). The sequence was initiated by the 1 January 1996 Tomini earthquake (M_w = 7.9) on the western edge of the Minahassa thrust and took place in three phases:

1. The initial phase was a classical thrust earthquake sequence propagating eastward along the Minahassa thrust for about two thirds of its length up to the Gorontalo fault (Figure 1).

2. The second phase started when seismicity jumped from the east-west Minahassa thrust to the south trending Palu fault and propagated southward. Two earthquakes with magnitude $M_w > 6$ occurred on or near the fault (21 May 1998 M_w 6.6 and 10 October 1998 M_w 6.0.) The first quake was located very close to the fault trace, and its CMT mechanism is clearly strike-slip, despite the fact that neither plane aligns well with the strike of the Palu fault. The depth and mechanism of the second quake are not well constrained, but its southeast dipping shallow plane and southeast oriented slip vector suggest that it is a thrust event (Figure 1).

3. Once the northwest corner of the Sula block has moved toward the north, the southeast corner of the same block produced the largest earthquake recorded in this area (M_w = 7.7, possibly on the south branch of the Sula-Sorong

[1]Ecole Normale Suprieure, Centre National de la Recherche Scientifique, Paris, France.
[2]Now at Laboratoire de Gophysique Interne et Tectonique, Université Grenoble, France.
[3]Delft Institute for Earth-Oriented Space Research, Delft, Netherlands.
[4]Rensselaer Polytechnic Institute, Troy, New York, USA.
[5]School of Computing, University of Canberra, Canberra, Australia.
[6]Scripps Institution of Oceanography, University of California, San Diego, La Jolla, California, USA.
[7]National Coordination Agency for Surveys and Mapping, Cibinong, Indonesia.
[8]Institut Teknologi Bandung, Bandung, Indonesia.
[9]Also at National Coordination Agency for Surveys and Mapping, Cibinong, Indonesia.
[10]Department of Survey and Mapping Malaysia, Kuala-Lumpur, Malaysia.

0148-0227/02/2001JB000377$09.00

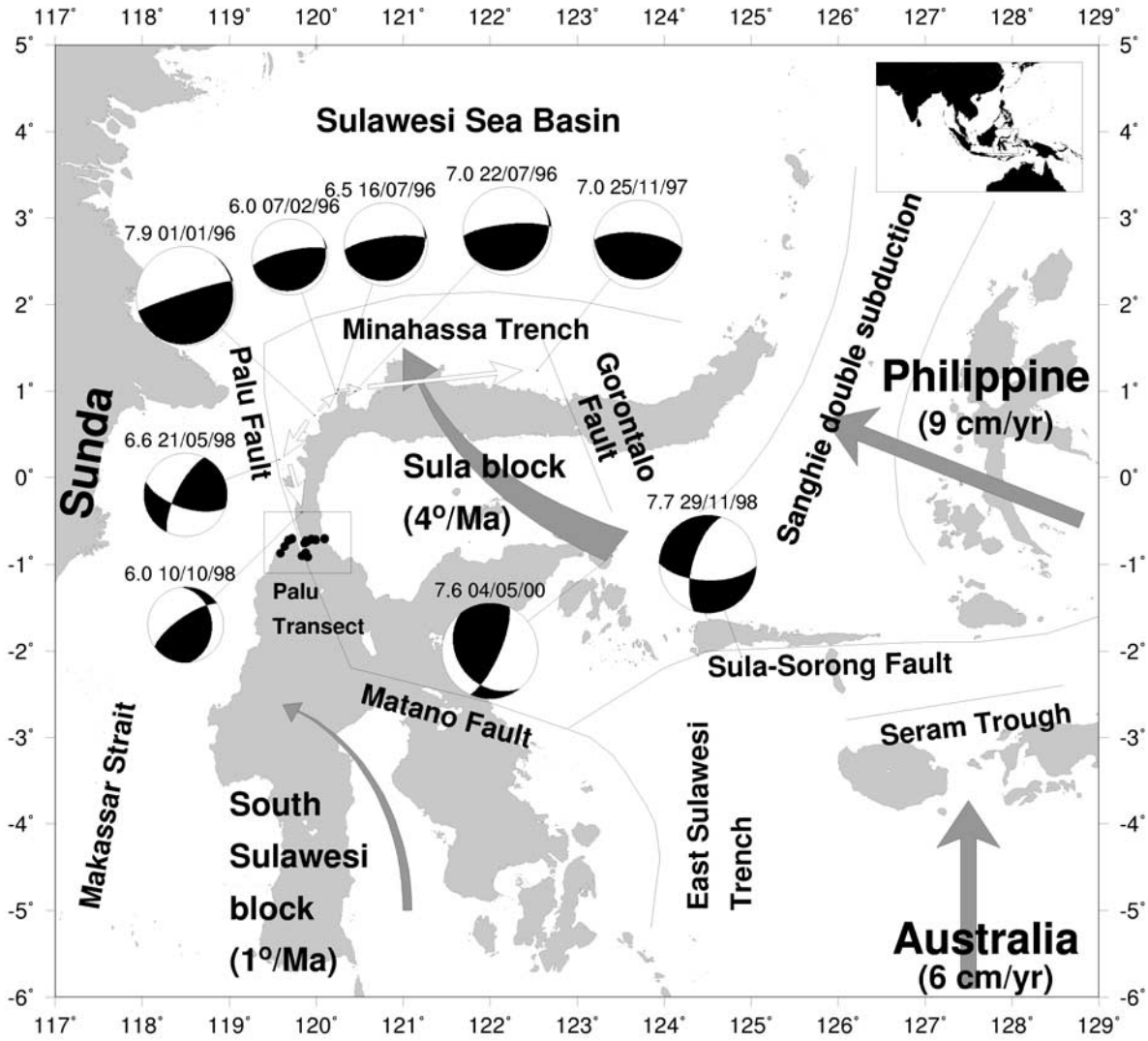

Figure 1. Tectonic setting of the triple junction area. Inset (top right corner) for reference. Straight arrows show the magnitude and direction of the Australian and Philippine plates velocities relative to Sundaland. Curved arrows depict the rotation of the Sula block toward the Minahassa trench, and the associated counter rotation of the South Sulawesi block relative to Sundaland. Focal mechanisms are from CMT catalog and depict only earthquakes of magnitude larger than 6 between 1 January 1996 and 1 June 2000. Propagation of seismicity is indicated by white arrows.

fault). More recently, another large event (4 May 2000 M_w 7.5) occurred in a former seismically quiet area, near the ophiolite belt of the old Sula thrust (Figure 1).

[4] Focal mechanisms and depths of the Palu fault sequence earthquakes are not well constrained in the CMT catalog. Therefore we reestimated those by performing a body wave inversion of *P* and *SH* wave seismograms recorded by the Incorporated Research Institutions for Seismology (IRIS) digital network. Using the algorithm of [*Nabelek*, 1985], we inverted for the best double couple focal mechanism, the scalar moment, the source time function and the centroid depth. To avoid upper mantle and core arrivals, we used teleseismic stations in the range 30° to 90°. The velocity structure near source and beneath the stations was approximated by a half-space with standard upper mantle wave speeds. In order to have the same reference instrument response at all stations, individual instrument responses were removed from the seismograms and all were convolved with a common instrument response. Seismograms were integrated to displacement and band passed with a third-order Butterworth filter between 1 and 50 s.

[5] The result for the first quake yields almost pure left-lateral strike-slip mechanism on a plane trending 190° to 200° (dip of 73.6, rake of 19.9), better aligned with the close to N-S strike of the fault at this latitude (Table 1). The depth remains difficult to determine but can be constrained between 20 and 30 km. Our modeling of the second earthquake, which was actually two events with equivalent magnitude separated by 3 min, confirms their thrust com-

Table 1. Earthquake Parameters

Date	NEIC			CMT						This Study			
	Location Lat, Long	M_w	Depth km	Plane 1			Plane 2			Depth, km	Plane		
				Strike	Dip	Rake	Strike	Dip	Rake		Strike	Dip	Rake
1 Jan. 1996	0.73, 119.93	7.9	24	36	6	54	252	85	94				
7 Feb. 1996	1.02, 120.19	6.1	13	61	14	75	257	76	94				
16 July 1996	1.02, 120.25	6.6	33	63	14	71	262	76	95				
22 July 1996	1.00, 120.45	7.0	33	57	14	63	264	77	96				
25 Nov. 1997	1.24, 122.54	7.0	24	98	21	93	275	69	89				
21 May 1998	0.21, 119.58	6.6	33	108	64	160	207	72	28	20–30	195	74	20
10 Oct. 1998	−0.40, 119.84	6.0	33	355	31	35	235	73	116	10–20	250	94	96
29 Nov. 1998	−2.07, 124.89	7.7	33	92	63	−28	196	65	−150				
4 May 2000	−1.11, 123.57	7.6	26	142	32	32	24	74	118				

ponent and constrains their depth to between 10 and 20 km, which is too shallow for the Minahassa trench. Therefore, while it is plausible that the first quake ruptured the fault, except that there is a significant difference in strike, it is clear that the double event did not. The structure on which they occurred in the vicinity of the fault is not documented.

[6] Interaction of the Minahassa trench and Palu fault area is investigated here through Coulomb stress studies and GPS measurements. Interaction between the northwest and southeast corners of the Sula block is quite speculative because the distance between them is so large (around 700 km) that the increase of stress computed by elastic half-space models is negligible. Thus the physical mechanism remains unclear, but a plausible description for such long distance interaction between earthquakes is given by *Chery et al.* [2001].

2. GPS Measurements

[7] GPS measurements were carried out at least once every year on a fault-normal profile in the Palu area from 1992 to 1999 [*Stevens et al.*, 1999; *Walpersdorf et al.*, 1998b]. Each year the two end sites of the profile were measured continuously throughout the whole campaign, while the intermediate transect sites were occupied for 6 to 12 hours sessions. Campaigns usually lasted between 5 and 7 days and each site were occupied for 1 to 4 sessions. The solution used in this work is computed using the GAMIT/GLOBK software [*King and Bock*, 1999; *Herring*, 1999]. Measurement sessions were reduced to daily positions using the L3 Ionosphere free combination and fixing the ambiguities to integer values. We used improved orbits computed at Scripps institution of Oceanography (SIO) [*Fang and Bock*, 1995] prior to 1994 and precise orbits from the International GPS Service for Geodynamics (IGS) afterwards [*Beutler et al.*, 1993]. We also used IGS-01 phase center model for modeling of antenna phase center variations. We do not use externally determined meteorological data but rather use the data themselves to estimate tropospheric delay parameters at each site (one every 3 hours). Every year, average horizontal baseline repeatabilities (scatter about the root mean square value) were of the order of a few millimeters for most baselines. Repeatabilities steadily improved from a high of 12–15 mm in 1993 (1992 being slightly better), when the global and regional tracking network was much sparser, to around 8 mm in 1994 and then to about 4 mm for the 1996 campaign. Thanks to the improved tracking network, the inclusion of transect measurements into regional campaigns and more often repeated longer sessions, the current (1999 for this work) repeatability is about 2 mm.

[8] Solutions in a consistent reference frame were obtained by including data from the permanent IGS network stations [*Neilan*, 1995] in our daily solutions. These data were combined with the local data in one single solution into a loose system using Helmert-type transformations in which translation, rotation, scale and Earth orientation parameters (polar motion and rotation) are estimated. The reference frame is then defined by minimizing the departure from a priori values, here International Terrestrial Reference Frame (ITRF) 97 [*Boucher et al.*, 1999], of the positions and velocities of a set of well determined stations. For the reference frame realization we used an increasing number of IGS stations as they became operational, ranging from five stations (KIT3, TAIW, TIDB, TSKB, YAR1) for the earlier epochs (1992–1993), to more than 10 stations in 1999. The misfit to those fiducial stations is 1 mm for positions and 0.7 mm/yr for velocities. Such small values indicate that local velocities are consistently computed in a stable reference frame.

[9] Additional data from local Sulawesi campaigns (1997 and 1999) and regional data from the GEODYSSEA campaigns in Southeast Asia (1994, 1996, 1998) [*Simons et al.*, 1999; *Michel et al.*, 2001] were also used to improve site positions and define a local Sundaland reference frame. Velocities in ITRF97 are rotated about a pole that minimizes the velocities at regional sites within Sundaland platelet. In this reference frame, Palu transect stations show velocities aligned with the Palu fault direction at this latitude, and increasing from west to east. A horizontal translation vector, equal to the velocity of station PALU (PL15), is then substracted from all transect stations. Doing so, we neglect the small velocity gradient (less than 1 mm/yr per 10 km) that should be present in the eastern part of the transect, due to the variable distance between the sites and their common block rotation pole (Sulawesi northern arm pole, 700 km away).

[10] Figure 2 show the velocities across the Palu fault in this local reference frame before (white arrows) and after (black arrows) the 1 January 1996 Tomini earthquake. We excluded from these the 1996 measurements, as they are affected by coseismic and postseismic deformations as demonstrated in this study. The earlier measurements (1992–1995), identical to those of *Stevens et al.* [1999], are less precise than the latest measurements (1997–1999). Concentrating on the along-strike velocity component, both

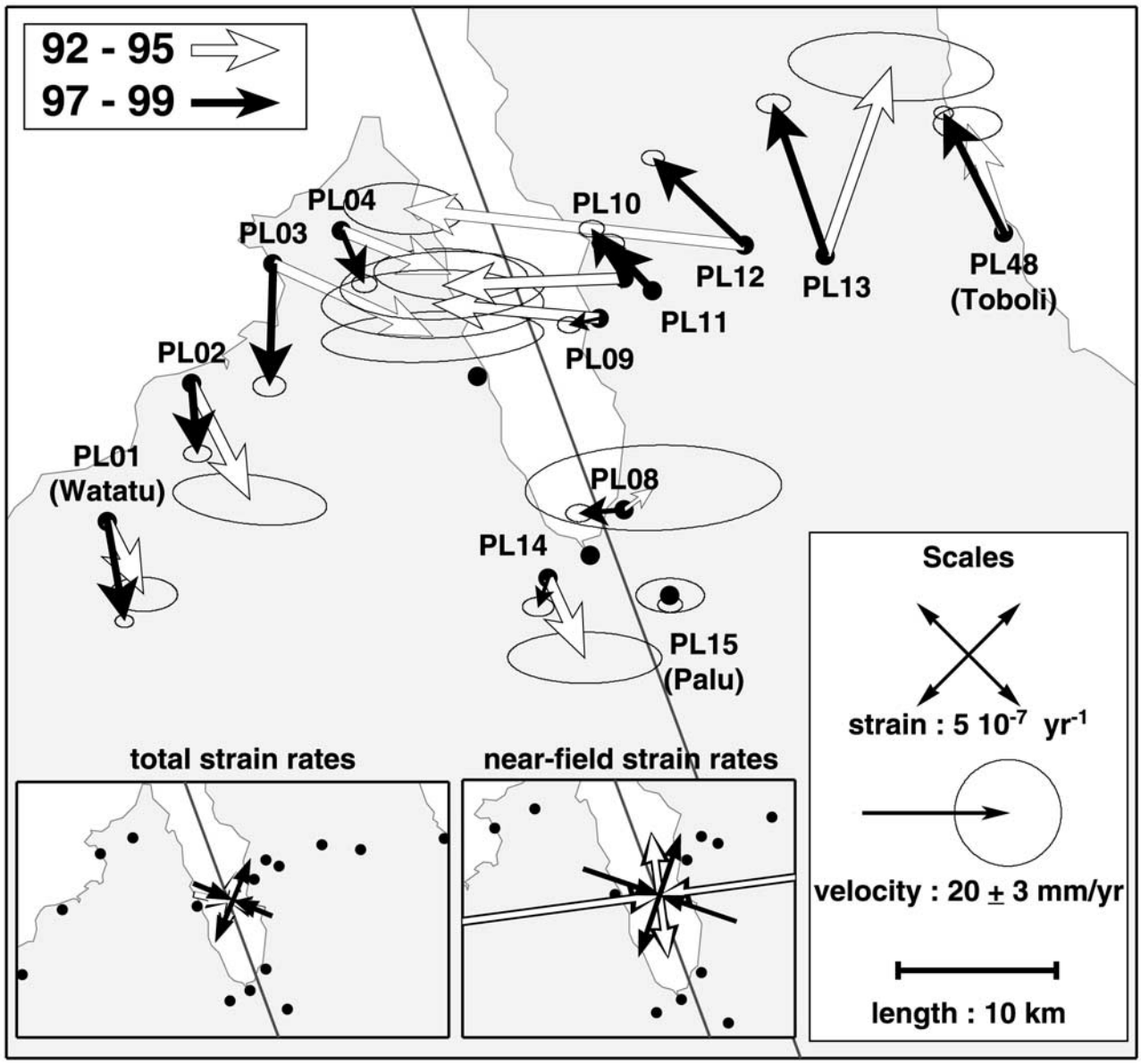

Figure 2. Velocities of the Palu transect stations in local Palu reference frame (see text for more complete explanation). White arrows are for the velocities inferred from 1992, 1993, 1994, and 1995 campaigns (before the 1 January 1996 Tomini earthquake). Black arrows depict the velocities obtained from 1997, 1998, and 1999 measurements (after the earthquake). Error ellipses show the 95% confidence level. The insets show the strain rates computed for the same periods, using the whole network (left inset) or using only the near-field stations which exhibit the higher east-west changes (middle inset).

sets of measurements show the typical distribution of slip across a locked fault (maximum of shear strain rate near the fault trace), with a locking depth of 5 to 15 km and a far-field velocity of about 40 mm/yr, consistent with *Stevens et al.* [1999]. As already noted by *Stevens et al.* [1999], the maximum shear is not centered on the geological fault trace [*Bellier et al.*, 1998], but located 10 km farther east, below Palu city. Superimposed on the along-strike motions, the preearthquake measurements at near-fault sites show strong contraction across the fault, while the recent measurements (1997–1999) do not show this compression. This feature could simply come from high east-west uncertainties of the earlier measurements. In particular, erroneous ambiguity resolution would mostly map in the longitude determination. Nevertheless, earlier stage of intense contraction is consistent with unexpected extension across the fault detected by the 1995–1997 measurements [*Walpersdorf et al.*, 1998b]. This coseismic and postseismic extension partly compensated the prior contraction and lead to a deformation regime closer to strike-slip motion on average. Figure 3 shows that the extension after 1 January 1996 compensated only part of the prior contraction. Continuous monitoring of future motions should enable us to see whether a return to contraction is observed and if this could be a repetitive pattern related to the loading-unloading cycle. The coseismic extension period could also be related to the possible

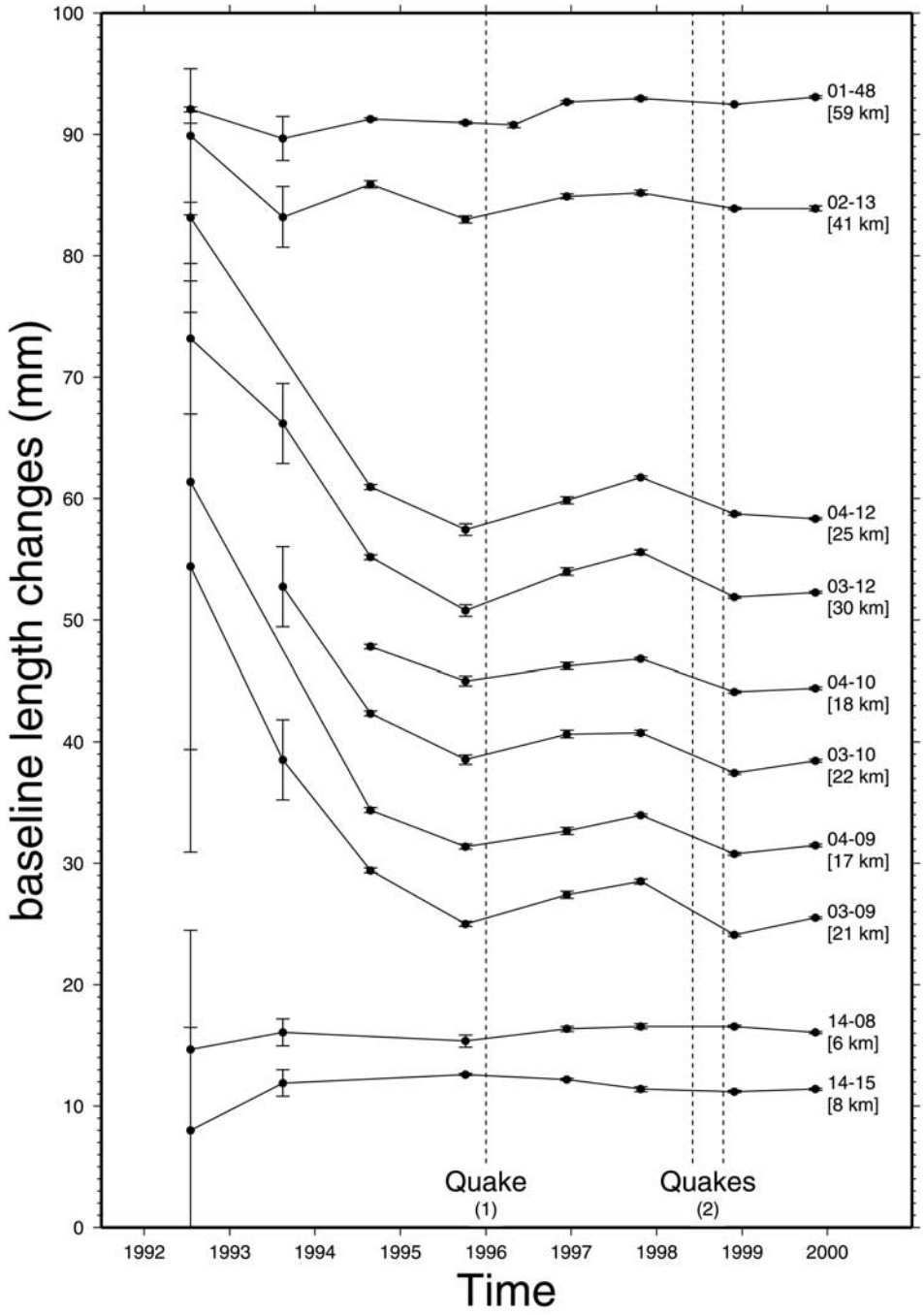

Figure 3. Time dependence of baseline length changes across the Palu fault. Solid symbols with error bars show the epoch measurement values with their associated uncertainties (1σ). The numbers on the right indicate which sites are considered for a particular baseline: PL08, 14, 15 for very short baselines across the fault; PL03, 04, 09, 10, 12 for near-field baselines; and PL01, 02, 13, 14 for far-field baselines.

unclamping effect detected by the Coulomb stress analysis (section 3).

[11] Strain rate tensors from the preearthquake and post-earthquake data allow us to determine whether the change in contraction is significant. Using the whole network, we find regional principal horizontal strain rates are not significantly different before and after the earthquake: 207 and −244 nstrain/yr (±100) with the maximum compressional strain axis oriented 102° (±25°) before 1 January 1996 and 311 and −291 nstrain/yr (±20) oriented 113° (±2°) after 1 January 1996 (Figure 2). The earlier values are roughly compatible with a left-lateral shear on a plane trending N33 W, which is approximately the direction of the Palu fault. Large uncertainties and the fact that far-field data show little contraction account for the misfit of the pre-1996 data to a uniform strain model. The later values are almost pure shear on a plane striking N22°W, very close to the N15°W Palu fault strike. Computations based on the near-field data only (two points

removed at both ends of the transect), give very different estimates: 435 and −2410 nstrain/yr (±300) oriented 82° before 1 January 1996 and 441 and −557 nstrain/yr (±25) oriented 109° after 1 January 1996 (Figure 2). From these numbers it is clear that while the far-field data show only a slight and maybe insignificant rotation of the principal strains toward pure shear, the near-field data show a large change in compression across the fault. The compression seen before 1 January 1996 is not present afterward.

[12] Another way of estimating how well the data are fit is to examine station positions as a function of time Figure 3, rather than use their linear velocity over a given period of time. With usual geodetic tools, relative baselines (distances between stations) are estimated more precisely than individual station positions. In addition, baseline lengths are free of errors introduced by unaccounted reference frame translations and rotations. Because most baselines cross the fault at high angles, their length variations are more representative of changes in motions perpendicular to the fault. The short baselines (PL08-PL14, PL14-PL15) 20 km south of the main transect, hardly show any change, especially given the larger uncertainty of the earlier epochs. The near-field baselines (ranging from PL04-PL09 = 17 km to PL03-PL12 = 30 km) all show a common tendency: a change of trend around 1996. Rapid shortening prior the Tomini earthquake is replaced by lengthening afterwards. The total magnitude of the shortening is not well constrained given the large uncertainties of the 1992 and 1993 epochs. Nevertheless, the first 3 epochs are well described by a linear velocity. Far-field baselines (PL02-PL13 = 41 km, PL01 to PL48 = 60 km) show little change (within the estimated uncertainties) throughout all epochs. Nevertheless, the longest baseline (PL01-PL48) measured in early 1996 shows a small but significant step later in 1996.

[13] To explain these measurements we consider two possible scenarios:

1. The change in near-fault strain rates is real and related to the 1 January 1996 Tomini earthquake. It is related to small but detectable motions perpendicular to the fault in the far-field (PL01-PL48), and large motions less precisely measured in the near field. The physical mechanism for such large and localized strains at the surface remains to be explained.

2. Contraction in the near field was over estimated due to errors in the earlier measurements, and therefore the change in surface strain near the Palu fault is also overestimated.

[14] Nevertheless, however unreliable the near-field data may be, the end points of the transect also see some of this change in motions perpendicular to the fault (with a much reduced amplitude) (Figures 3 and 4, middle). Therefore we think transient motions perpendicular to the fault indeed occurred in relation to the 1 January 1996 Tomini earthquake. The amplitude of these motions remain uncertain, but their existence seems certain.

[15] Figure 4 shows the Watatu-Toboli baseline (PL01-PL48) components versus time for the full period 1992–1999. Those two points are the reference stations for our measurement campaigns and therefore are observed much more than any other. Each year, we measured them simultaneously and continuously (24 h/d) for 5–10 days, therefore spanning different tropospheric conditions, obtaining the best possible sky coverage, and averaging possible multipath effects. This operating scheme allows us to obtain at all epochs since 1995 significant repeatabilities no larger than a few millimeters on this baseline. In addition, since 1996, the geodetic monuments at these sites (1 m deep concrete benchmark in flat soil, anchored at 2 m depth by iron rods) were equipped with specially designed markers allowing forced centering of the GPS antennas, avoiding tripod and optical tribrachs, and yielding a submillimeter accuracy of recentering. Therefore small horizontal position variations at those sites cannot be attributed to setup errors. Assuming that the fault strikes N15°W, the motion of Toboli relative to Watatu is separated into its three components: parallel and perpendicular to the fault in the horizontal plane, and vertical. Being close to the north-south direction, the fault parallel component is the most precisely determined and very clearly shows three distinct periods (Figure 4, top): (1) an initial period from 1992 to 1995 (4 epochs) of steady displacement at a rate of 25 mm/yr, (2) an intermediate period between 1996 and 1997 (3 epochs) at a rate higher than 60 mm/yr, and (3) the present period from 1997 to 1999 (3 epochs), at the original rate. The intermediate period clearly followed the 1 January 1996 Tomini earthquake.

[16] A first anomalous offset of about 20 mm superimposes itself on the normal trend between November 1995 and April 96 measurements. This step displacement is the sum of the instantaneous coseismic displacement generated by the earthquake at 80 km distance and postseismic creep during the following 4 months (January to April). This ''coseismic'' period has no reason to exhibit linear motions. For an elastic rheology, the stress step should produce a step in displacement, not a change in velocity. If the rheology is viscoelastic, we would expect to see an exponential relaxation from a displacement appropriate for the unrelaxed modulus to a displacement appropriate for the relaxed modulus. The early stages of the relaxation could appear linear. Elastic dislocation model (following *Okada* [1992]) matches well this first offset [*Gomez et al.*, 2000; *Walpersdorf et al.*, 1998b].

[17] The second anomalous displacement, which again adds 20 mm to the interseismic trend between April 1996 and December 1996, is purely postseismic since no other earthquake with the adequate magnitude/distance ratio occurred in the area within this time span. Elastic modeling of strain generated by the M_w = 7, 22 July 1996 event farther away on the Minahassa trench, shows insignificant motion at both Watatu and Toboli. Silent postseismic deformation release on the trench has also been observed on the Japan trench after the 1994 Sanriku-Haruka-Oki earthquake sequence [*Heki*, 1997]. Similar to the Japanese case, the postseismic relaxation lasted for about one year, since the December 1997 measurements (Figure 4, top) clearly indicate a return to normal trend.

[18] The coseismic and postseismic displacements at this particular location of Toboli (relative to the stable block represented by Watatu) are about the same. If the source of the postseismic motion has the same location as the coseismic source (silent fault after slip or slow earthquake on the same fracture plane), then it appears that the postseismic slip approximately equals the coseismic. Obviously, this claim does not hold if we consider viscoelastic relaxation or a source of deformation different than the coseismic. It is

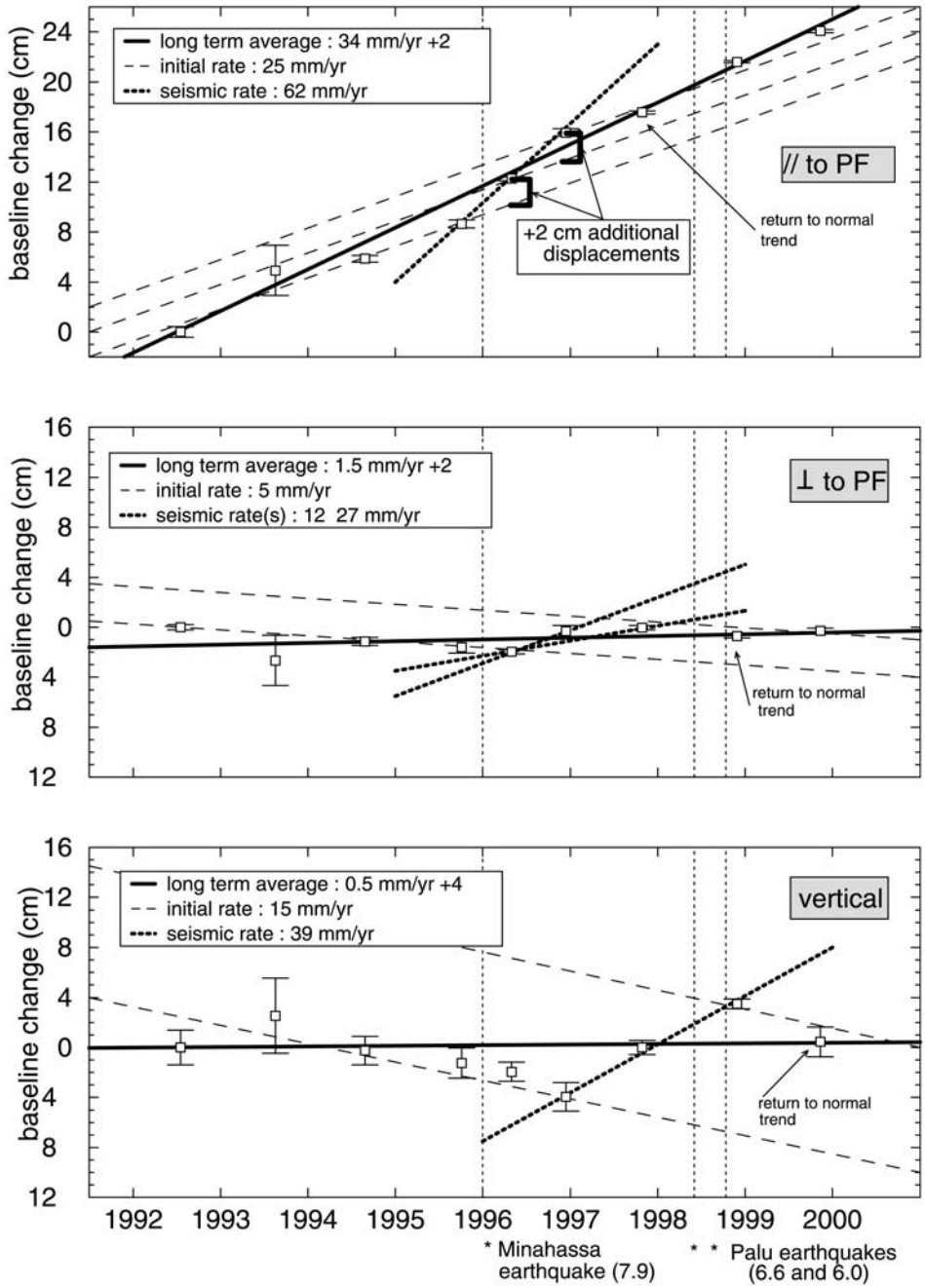

Figure 4. Evolution of the Watatu-Toboli baseline across the Palu fault. (top) Component parallel to the fault (along strike), (middle) component perpendicular to the fault (normal component), and (bottom) vertical component. Scales are years for time and centimeters for displacements. Squares with error bars show the epoch measurement values with their associated uncertainties (1σ). The thick lines give the long-term average rates obtained for all epochs. Dashed lines indicate the initial rates inferred before the 1 January 1996 Minahassa earthquake (open squares). The dotted thick lines depict the intermediate periods of anomalous rates following the 1 January 1996 earthquake (solid squares), which start and end at different epochs for the different components. The thin vertical dotted lines and the legend strings at the bottom of the plate mark the dates of the earthquakes in the area of the measurements.

difficult to discriminate between the two hypothesis without measurements at other locations closer to the Minahassa trench during the intermediate period (early 1996 to late 1997). Using the standard definition of a characteristic Maxwell time for viscoelastic relaxation ($t = \eta / E$), and using $t = 1$ years and $E = 3 \times 10^{10}$ Pa for the shear modulus, we find a viscosity η of about 10^{18} Pa s for the lower crust or upper mantle in the area. Such a value is reasonable within a subduction domain and is also very similar to results from California [*Pollitz et al.*, 2001], but again, other

mechanisms such as a slow earthquake or afterslip on the Minahassa trench cannot be ruled out. No matter what, the hypothesis that aseismic slip was triggered on the Palu fault can be rejected since the near-field points on either side of the fault do not show relative motions parallel to the fault during the intermediate period, other than the expected 5 mm/yr of interseismic deformation.

[19] Although less precise, the normal and the vertical components show similar trends (Figure 4, middle and bottom). Shortening and subsidence of the eastern part from 92 to 96 is followed by a brief, rapid period of opening (normal component) and uplift from 1996 to 1998, and back to the original trend since. The normal and vertical components are delayed with respect to the strike-slip component. Therefore, changes in trends start and end at different times in Figure 4. In particular, the intermediate period of opening started only after April 1996, when the increase of the along-strike component started directly after January 1996 earthquake. This intermediate period of opening also lasted longer since the December 1997 measurements do not show a return to the initial trend, unlike the along-strike component. Those three epochs (early 1996, late 1996, and late 1997) clearly do not lie on the fault-perpendicular inter seismic trend. Whether they define one single 18 month linear rate, two different linear trends, or a more complex relaxation curve, is impossible to assess with three points only. It is only after the normal component returned to the initial interseismic trend that the first Palu fault earthquake occurred. This delay is possibly related to fluid migration within the fault plane, triggered by a decrease in the fault normal stress (unclamping). If so, the time delay could be related to the characteristic time of fluid migration. The hypothesis of fluid migration triggered by unclamping is discussed in section 3.

[20] The average slip rate over the 7 years period (including all epochs) is 34 ± 2 mm/yr. This is not the total far-field rate across the Palu fault since the baseline lies within the zone of elastic strain accumulation due to the fault being locked. Following *Savage and Burford* [1973], we find a larger long-term total slip rate of between 38 and 42 mm/yr. Because this rate includes the 1996 measurements, it is affected by the intermediate period. Removing the coseismic and postseismic offsets leads to rates of 28 mm/yr on the baseline and 30–35 mm/yr on the fault. This rate is probably closer to the long-term interseismic and matches the estimate based on rigid rotation of the Sulawesi northern arm (4°/Myr about a pole located at its northern tip) and earlier GPS estimates [*Stevens et al.*, 1999].

3. Coulomb Stress Computations and Quake Triggering

[21] We use the Coulomb failure function, CFF = $|\tau| + \mu\sigma$, in which τ is the shear stress, σ is the normal stress, and μ is the friction coefficient, to estimate if a given earthquake has brought nearby faults closer to or farther from failure [*Harris*, 1998]. If CFF is positive, then the change in shear stress is "dragging" the fault toward motion. Since the initial state of stress on the fault is unknown, we consider here the change of CFF: $\Delta CFF = \Delta|\tau| + \mu\Delta\sigma$. In this study we neglect the effect of cohesion and pore pressure, the implication being just a correction of the friction coefficient which in fact is largely unknown.

[22] With this simple failure criterion we estimate stress transfer by an earthquake using the slip in a rectangular dislocation in an elastic half-space [*Okada*, 1992]. Knowing the earthquake's moment and the fault area that ruptured during the earthquake, and assuming some typical values of the elastic modulus (Poisson ratio of 0.25, shear modulus of 3×10^{10} Pa), we derive the coseismic slip on the fault and estimate the stress transfer by the earthquake on the fault. Assuming a value of μ ($\mu = 0.4$), we calculated Δ CFF at every point in the elastic half-space. The parameters (magnitude, orientation, depth, rake and dimensions of the fault) used for the main shock come from *Gomez et al.* [2000]. For our computations, we use the DLC dislocation code [*Reasenberg and Simpson*, 1992; *Simpson and Reasenberg*, 1994].

[23] Figure 5 shows Coulomb stress increase generated by the 1 January 1996, $M_w = 7.9$, earthquake over a selected area of Sulawesi. Keeping in mind that their occurrence on the Palu fault itself is not certain, both of the so-called "Palu fault aftershocks" (21 May 1998 M_w 6.6 and 10 October 1998 M_w6.0) occurred in areas where the Coulomb stress was much increased (4.5 bars) for the first one and still significantly increased (0.7 bars) for the second one.

[24] The regularly spaced gridded "beach balls" indicate the preferred mechanism for an earthquake at this place. That is, an earthquake with this focal mechanism would use 100% of the Coulomb stress increase at this location. We suggest that earthquakes should occur where a fault available for rupture is compatible with the preferred mechanism. The first aftershock did not take place farther north on the Palu fault where stress increase was larger, but the preferred mechanism is not compatible with the fault there. Therefore it took place within the area of stress increase, but only where the preferred mechanism was compatible with the existing fault. In this area, the preferred mechanism exhibits a strike-slip component like the actual one (see the gridded beach ball immediately left of the observed one). The second aftershock has a smaller stress increase to take advantage of, and its mechanism is not well aligned with the preferred mechanisms around (left-up and left-down).

[25] For a rigorous comparison, the regional preexisting stress pattern should be taken into account, since the aftershock will release both preexisting and main shock-induced stresses in the area. Unfortunately, the preexisting stress level is largely unknown in this area due to the lack of local seismic stations and the complexity of the local structure. However, seismicity as recorded by global and local Indonesian networks indicates a low level of shallow seismic activity in central Sulawesi [e.g., *McCaffrey and Sutardjo*, 1982; *Beaudouin*, 1998]. Nevertheless, in this case the match with the increase of Coulomb stress alone is already reasonable. It shows that in at least the case of the first Palu fault afterschock, that fault was brought closer to failure by the 1 January 1996 earthquake.

[26] The earlier aftershocks which occurred along the trench during 1996 also took place in an area of significant Coulomb stress increase. The most favored mechanism there is also fully compatible with the subhorizontal fault plane along the trench, suggesting that those events were also triggered by the main shock.

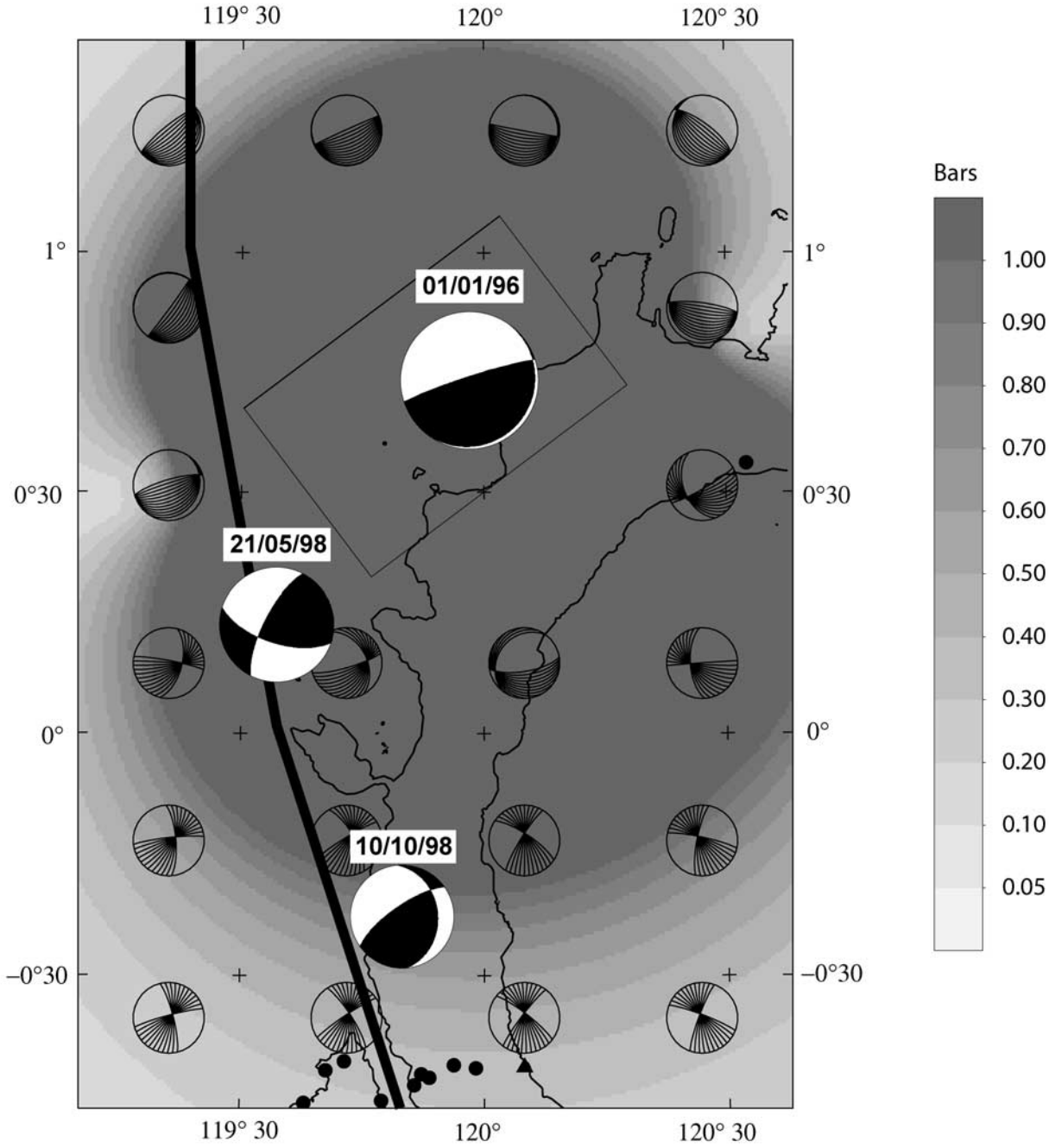

Figure 5. Coulomb stress transfer generated by the M_w7.9 1 January 1996 Minahassa Earthquake, computed at 15 km depth on optimally oriented planes. The color scale is in bars and linear. Full ''beach balls'' depict the CMT focal mechanisms for the main shock and the two aftershocks, when the gridded beach balls depict the focal mechanism of the earthquake most compatible with the Δ CFF at specific locations. The rectangle shows the assumed rupture plane of the main shock. The two aftershocks took place in an area of significant Coulomb stress increase.

[27] Figure 6 shows stress increase on the Palu fault plane computed for a friction coefficient of 0.4 on the fault plane. Both aftershocks are again within an area of Coulomb stress increase, which does not go deeper than 20–25 km (Figure 6a), and where the stress loading favors left-lateral mechanisms (Figure 6b), which are the expected mechanism for a left-lateral fault. The two aftershocks are also in an area where the normal stress increases (Figure 6c), which means opening according to the sign convention. Such an unclamping may also have induced fluid migration into the fault plane itself. Presence of overpressured fluids in the fault plane is known to change the normal stress by

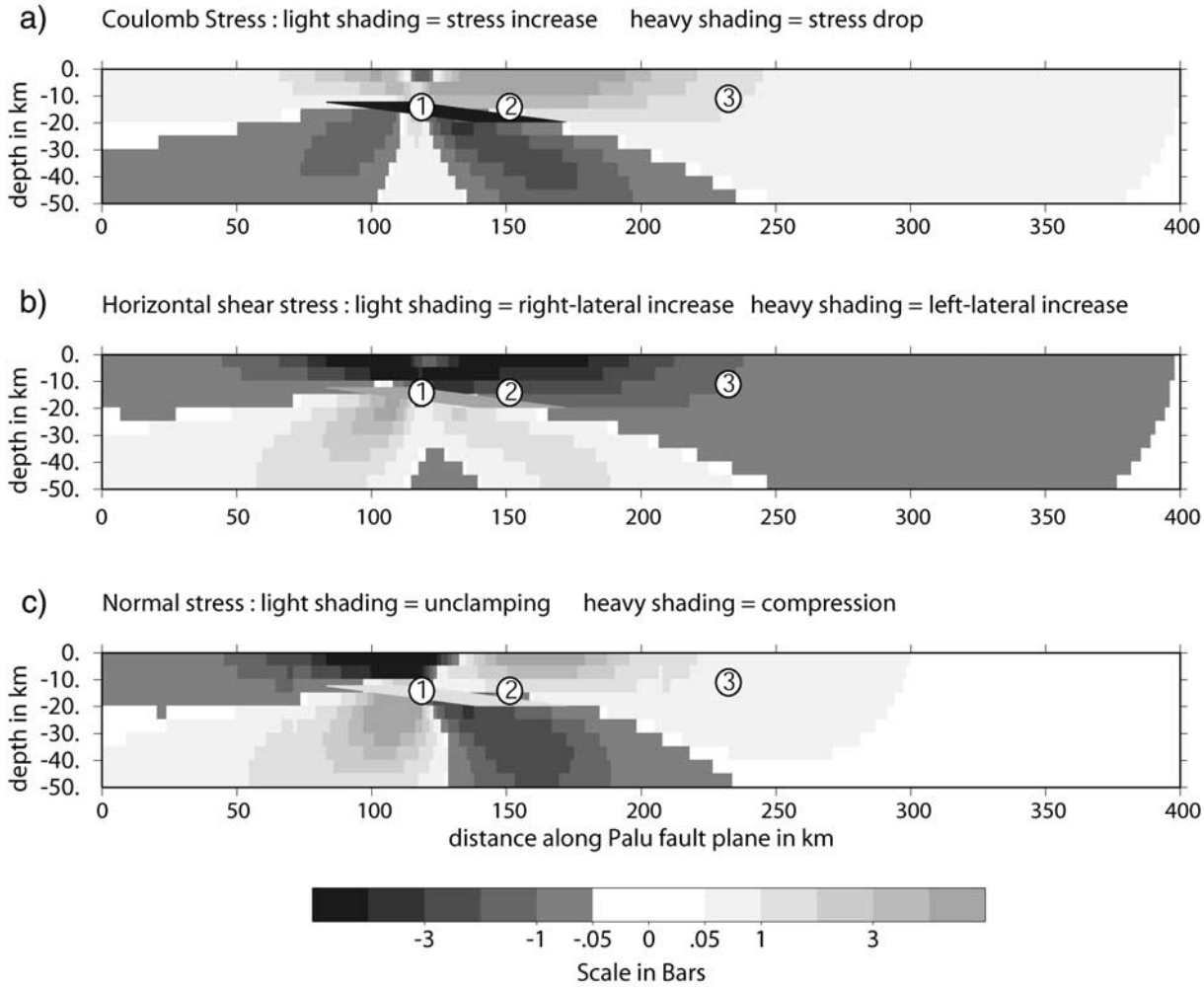

Figure 6. Stress increase generated by he M_w7.9 1 January 1996 Minahassa earthquake, computed along the Palu-Koro fault plane with friction coefficient of 0.4. (top) Coulomb stress, (middle) shear stress (parallel to the fault plane), and (bottom) normal stress (perpendicular to the fault plane). Scale is in bars and color contouring is logarithmic. The numbers in circles indicate the positions of (1) the 1 January 1996 main shock and (2) the first 21 May 1998 and (3) the second 10 October 1998 aftershocks. The two aftershocks took place in an area where the Coulomb stress was increased, left-lateral shear stress was added, and unclamping was effective.

changing the pore pressure in such a way that it probably facilitate it's rupture.

[28] This phenomenon may explain the time delay of the intermediate period displacement of the normal component (Figure 4). Coulomb stress modeling indicates that the Tomini earthquake generated immediate unclamping on the Palu fault, but this did not generate instantaneous motions perpendicular to the fault: the April 1996 measurement clearly lies along the normal trend (Figure 4, middle). Our interpretation is that unclamping may have triggered fluid migration in the fault plane, which in turn may have generated an opening motion across the fault.

[29] Fluid migration in the fault plane may also explain why it took 2.5 years to rupture the fault area after the initial earthquake, and why it did not rupture within the 1.5 years that the additional postseismic along-strike deformation occurred. Using a classical diffusion law where the migration distance is proportional to the root square of time $(d = \sqrt{Ct})$, and typical values for the poroelastic constant C in this material (around 1 m^2 s^{-1}) [*Etheridge et al.*, 1984], we find d = 9 km for a period of 2.5 years. This distance of 9 km matches quite well the locking depth of the fault. Therefore it may be speculated that the fault ruptured only after the full plane depth was penetrated by fluids. This occurred around the same time the normal component ''intermediate'' period opening finished, roughly 1 year after the end of the along-slip intermediate period increase.

[30] This idea of time delay controlled by fluid migration remains hypothetical. In particular, if the unclamping induces fluid flow by lowering the pore pressure in the fault, thus setting up a pressure gradient, the fluid will move into the fault zone until the pressure gradient is gone. At this point

the pressure in the fault zone will be the same as outside the fault zone and the same as it was before the unclamping. Then a subsequent elevation of the pore pressure, or an increase of shear stress is needed to drive the system toward failure beyond immediate effect of the unclamping.

4. Conclusion

[31] Coulomb stress analysis shows how the magnitude 7.9, 1 January 1996 earthquake in northwest Sulawesi could have triggered large aftershocks in the area. Moreover, GPS measurements also detected both the instantaneous coseismic displacement and transient motions associated with viscoelastic relaxation or afterslip. The Coulomb stress computations are in good agreement with the strain measured by GPS. In particular on the Palu fault where the strain generated by the Minahassa earthquake added to the long-term strike-slip accumulation and generated opening of the fault contrary to the long-term motion but in agreement with the orientation of the computed normal stress. This unclamping effect may be critical in triggering the Palu fault sequence since it lasted longer than the along strike component effect, as attested by the position of the November 1997 epoch (Figure 4). It was only after the maximum opening was reached that rupture occurred in the Palu fault area. Last but not least, the Palu fault poses an acute seismic hazard for the Palu city area since it will take the equivalent of a $M_w \sim 7$ or larger earthquake to release the accumulated strain over the past several decades at a rate close to 40 mm/yr [*Stevens et al.*, 1999]. The latest sequence of earthquakes on or near the northern part of the Palu fault did nothing else but increase the probability of an earthquake farther south in the near future.

[32] **Acknowledgments.** We are grateful to everyone involved in the long-term collaboration on the Palu-Koro GPS transect since 1992. Special thanks to all surveyors from BAKOSURTANAL and DSMM. SIO and RPI initiated the program supported by NSF grants EAR-9114349 and EAR-9114864. The bulk of this work has been achieved to a large part in the framework of the GEODYSSEA project under contract CI1*-CT93-0337 between the European commission and the GFZ in Germany. The most recent part has been achieved in a collaboration between DEOS and ENS for Europe, ITB Bandung and BAKOSURTANAL for Indonesia, and DSMM for Malaysia. We would also like to thank the anonymous reviewers of this manuscript and the JGR Associate Editor. Their detailed comments and writing suggestions greatly helped in improving this article.

References

Beaudouin, T., Tectonique active et sismotectonique du systme de failels dcrochantes de Sulawesi central, Ph.D. thesis, 343 pp., Univ. Paris-Sud, Orsay, France, 1998.

Bellier, O., T. Beaudouin, M. Sebrier, M. Villeneuve, I. Bahar, E. Putranto, I. Pratomo, M. Massault, and D. Seward, Active faulting in central Sulawesi (eastern Indonesia), in *GEODYSSEA Project Final Report*, edited by P. Wilson and G. W. Michel, *Sci. Tech. Rep. STR 98-14*, 276–312, GeoForshungZentrum, Potsdam, Germany, 1998.

Beutler, G., J. Kouba, and T. Springer, Combining the orbits of the IGS processing centers, in *Proceedings of IGS Analysis Center Workshop*, edited by J. Kuba, pp. 20–56, Geod. Surv. Div., Nat. Resour. Can., Ottawa, 1993. (Available at http://igscb.jpl.nasa.gov/overview/pubs.html).

Boucher, C., Z. Altamimi, and P. Sillard, The 1997 International Terrestrial Reference Frame (ITRF97), *IERS Tech. Note 27*, Obs. de Paris, 1999.

Chery, J., S. Merkel, and S. Bouissou, A physical basis for time clustering of large earthquakes, *Bull. Seismol. Soc. Am.*, *91*, 1685–1693, 2001.

Dziewonski, A. M., T.-A. Chou, and J. H. Woodhouse, Determination of earthquake source parameters from waveform data for studies of global and regional seismicity, *J. Geophys. Res.*, *86*, 2825–2852, 1981.

Dziewonski, A. M., G. Ekstrom, and M. P. Salagnik, Centroid-moment tensor solutions for July–September 1995, *Phys. Earth Planet. Inter.*, *97*, 3–13, 1996.

Etheridge, M. A., V. J. Wall, S. F. Cox, and R. H. Vernon, High fluid pressure during regional metamorphism and deformation: Implications for mass transport and deformation mechanisms, *J. Geophys. Res.*, *89*, 4344–4358, 1984.

Fang, P., and Y. Bock, Scripps Orbit and Permanent Array Center report to the IGS, in *IGS Annual Report*, edited by J. F. Zumberge et al., *JPL Publ., 95–18*, 213–233, 1995.

Gomez, J. M., R. Madariaga, A. Walpersdorf, and E. Chalard, The 1996 earthquake in Sulawesi, *Bull. Seismol. Soc. Am.*, *90*, 739–752, 2000.

Harris, R., Introduction to special section: Stress triggers, stress shadows, and implications for seismic hazard, *J. Geophys. Res.*, *103*, 24,347–24,358, 1998.

Heki, K., Silent fault slip following an interplate thrust earthquake at the japan trench, *Nature*, *386*, 595, 1997.

Herring, T. A., Documentation for the GLOBK software version 5.01, Mass. Inst. of Technol., Cambridge, 1999.

King, R. W., and Y. Bock, Documentation for the GAMIT GPS software analysis version 9.9, Mass. Inst. of Technol., Cambridge, 1999.

McCaffrey, R., and R. Sutardjo, Reconnaissance microearthquake survey of Sulawesi, Indonesia, *Geophys. Res. Lett.*, *9*(8), 793–796, 1982.

Michel, G., C. Reigber, M. Becker, H. Seeger, W. Simons, B. Ambrosius, C. Vigny, N. Chamot-Rooke, X. Le Pichon, P. Morgan, and S. Mattheussen, Crustal motion and block behaviour in SE Asia from GPS measurements, *Earth Planet. Sci. Lett.*, *187*, 239–244, 2001.

Nabelek, J., Geometry and mechanism of faulting of the 1980 El Asnam, Algeria, earthquake from inversion of teleseismic body waves and comparison with field observations, *J. Geophys. Res.*, *90*, 12,713–12,728, 1985.

Neilan, R., The evolution of the IGS global network, current status, and future aspects, in *IGS Annual Report*, edited by J. F. Zumberge et al., *JPL Publ., 95–18*, 25–34, 1995.

Okada, Y., Internal deformation due to shear and tensile faults in a half-space, *Bull. Seismol. Soc. Am.*, *82*, 1018–1040, 1992.

Pollitz, F., C. Wicks, and W. Thatcher, Mantle flow beneath continental strike-slip fault: Postseismic deformation after the 1999 Hector mine earthquake, *Science*, *293*, 1814–1818, 2001.

Reasenberg, P. A., and R. W. Simpson, Response of regional seismicity to the static stress change produced by the Loma Prieta earthquake, *Science*, *255*, 1687–1690, 1992.

Savage, J. C., and R. O. Burford, Geodetic determination of relative plate motion in central California, *J. Geophys. Res.*, *78*, 832–845, 1973.

Simons, W., B. Ambrosius, R. Noomen, D. Angermann, P. Wilson, M. Becker, E. Reinhart, A. Walpersdorf, and C. Vigny, Observing plate motions in SE Asia: Geodetic results of the GEODYSSEA project, *Geophys. Res. Lett.*, *26*(14), 2081–2084, 1999.

Simpson, R. W., and P. A. Reasenberg, Earthquake-induced static stress changes on central California faults, the Loma Prieta, California, earthquake of October 17, 1989—Tectonic processes and models, *U.S. Geol. Surv. Prof. Pap.*, *1550-F*, 55–89, 1994.

Stevens, C., R. McCaffrey, Y. Bock, J. Genrich, C. Endang, S. S. O. Subarya, Puntodewo, Fauzi, and C. Vigny, Rapid rotations about a vertical axis in a collisional setting revealed by the Palu fault, Sulawesi, Indonesia, *Geophys. Res. Lett.*, *26*(17), 2677–2680, 1999.

Walpersdorf, A., C. Vigny, P. Manurung, C. Subarya, and S. Sutisna, Determining the Sula block kinematics in the triple junction area in Indonesia by GPS, *Geophys. J. Int.*, *135*, 351–361, 1998a.

Walpersdorf, A., C. Vigny, C. Subarya, and P. Manurung, Monitoring of the Palu-Koro Fault (Sulawesi) by GPS, *Geophys. Res. Lett.*, *25*(13), 2313–2316, 1998b.

A. Lemoine, H. Perfettini, C. Vigny, and A. Walpersdorf, Ecole Normale Supérieure, CNRS, 24 rue Lhomond, F-75231, Paris Ceded 05, France. (vigny@geologie.ens.fr)

B. A. C. Ambrosius, W. J. F. Simons, and D. L. F. van Loon, Delft Institute for Earth-Oriented Space Research, Kluyverweg 1, 2629 HS Delft, Netherlands. (Wim.Simons@lr.tudelft.nl)

R. McCaffrey and C. Stevens, Rensselaer Polytechnic Institute (RPI), Troy, NY 12180, USA. (mccafr@rpi.edu)

Y. Bock, Scripps Institution for Oceanography, La Jolla, CA 92093-0225, USA. (bock@pgga.ucsd.edu)

P. Morgan, School of Computing, University of Canberra, College Street, Bruce, ACT 2616, Australia. (pjm@ise.canberra.edu.au)

P. Manurung and C. Subarya, National Coordination Agency for Surveys and Mapping (BAKOSURTANAL), Jl. Raya Jakarta-Bogor KM.46, Cibinong 16911, Indonesia. (geodesi@server.indo.net.id)

H. Abidin and J. Kahar, Institut Teknologi Bandung, Jl. Ganesha 10, Bandung 40132, Indonesia. (hzabidin@indo.net.id)

S. H. Abu, Department of Survey and Mapping Malaysia, Jl. Semarak, Kuala Lumpur MY-50578, Malaysia. (sbha@pc.jaring.my)